Far-field effects by arrays of oscillating wave surge converters and heaving point absorbers: a comparative study

Gael Verao Fernandez
Department of Civil Engineering, Ghent University
Technologiepark 904, B-9052, Ghent, Belgium
E-mail: gael.veraofernandez@ugent.be

Philip Balitsky
Department of Civil Engineering, Ghent University
Technologiepark 904, B-9052, Ghent, Belgium
E-mail: philip.balitsky@ugent.be

Nicolas Tomey Bozo
Centre for- Marine and Renewable Energy (MaREI), College University Cork
Beaufort Building. Environmental Research Institute. MERC Campus, Ringaskiddy, Ireland
E-mail: nicolas.tomey@ucc.ie

Vasiliki Stratigaki
Department of Civil Engineering, Ghent University
Technologiepark 904, B-9052, Ghent, Belgium
E-mail: vasiliki.stratigaki@ugent.be

Peter Troch
Department of Civil Engineering, Ghent University
Technologiepark 904, B-9052, Ghent, Belgium
E-mail: peter.troch@ugent.be

***Abstract*—Recent commercial developments and economical studies have shown that bottom-mounted pitching flaps and heaving point absorbers are principle candidates for deployment in commercial sized arrays. Much recent investigation has focused on the optimal configuration of arrays of Wave Energy Converters (WECs) but far fewer studies have focused on the far-field effects, that is the wave height modification in the area surrounding the WEC arrays. In this investigation we compare the far-field effects of bottom fixed flaps and heaving buoys for both a fixed bathymetry and a sloping bottom utilizing a recently developed coupling technique between the BEM model NEMOH and the wave propagation model MILDwave. A 9-buoy array of heaving buoys and a 5-WEC array of flaps of similar dimensions are simulated for different sets of regular wave conditions of varying wave periods. The magnitude of the effects in relation to their pacts on the surrounding coastline is discussed. Further, we discuss the advantages of modelling the realistic WEC array deployment using the presented coupling method.**

***Index Terms*—WEC array, WEC farm, hydrodynamic interactions, far-field effects, model coupling, BEM, mild-slope, MILDwave, NEMOH**

I. Introduction

Ocean Wave Energy is a promising source of clean electricity with the potential to significantly contribute in reducing the world's dependence on fossil fuels. However, wave energy conversion lags in technological and economic development behind other renewable energy sources such as wind and solar. It is the expectation of the wave energy industry that significant reductions in cost will enable its large scale deployment. Because of their operation in a highly energetic environment, most current wave energy devices cannot be scaled up individually like, e.g. bl,, a wind turbine. Consequently, in order for this technology to operate at grid scale, a deployment of a large number of devices in close proximity is necessary. Such an agglomeration is commonly termed a *wave farm* and is comparable in rated capacity to an offshore wind farm. A wave farm can consist of either hundreds of individual devices spaced far apart or groups of closely spaced devices commonly termed *Wave Energy Converter (WEC) arrays*.

Because of hydrodynamic interactions between the WECs, their layout in an array and farm will determine the total power output and by extension the economics of a wave energy project. These hydrodynamic interactions between WECs are often described as the *inter-array* effects in literature. The uptake and redistribution of wave energy will also have an impact on the surrounding coastline, in what is defined as *far-field* effect. The majority of existing studies have focused on the inter-array effect for the purpose of finding the optimal configuration for maximum wave energy uptake [1]–[3]. Those studies that have looked at the *far-field* effect have shown a significant impact, which may be more due to the coarse resolution of the models than to the real impact of the devices [4], [5]. A new approach which we use herein that seeks to rectify these setbacks couples models of different resolutions in which the wave interactions are modelled at high fidelity and then propagated out to the far-field in a lower-resolution model. Examples of this approach can be found in [6]–[9].

The aim of our paper is to investigate the impact of the WEC array far-field effects for a realistic deployment scenario using the newly developed coupling methodology first presented in [10]. For this purpose we choose two device types that show the most economic perspective, heaving buoys and pitching

bottom fixed flaps, the latter sometimes termed Oscillating Surging WECs (OSWECs). We consider the modification of the surrounding wave field for a staggered array of 9 heaving buoys and another array 5 pitching flaps placed in a varying bathymetry for a range of regular wave conditions. In this investigation the Boundary Element Method (BEM) solver NEMOH [11] is used to model the inter-array effects which are then coupled into the wave propagation model MILDwave [12], [13] that determines the far-field effects. The conventions of linear potential theory are assumed, as detailed in Sec. II.

II. Theoretical Background

A. Linear Potential Flow

This investigation assumes linear potential flow theory [14], a subset of linear wave theory that allows the flow velocity, v, to be expressed as the gradient of the potential, Φ (Eq. (1)).

$$v = \nabla\Phi \tag{1}$$

The assumptions underlying potential flow are the following:

- The flow is inviscid;
- The flow is irrotational;
- The flow is incompressible.

The standard assumption of linear theory that the motion amplitudes of the bodies are much smaller than the wavelength also applies. Linear potential flow theory has hitherto been utilized in a majority of the investigations into WEC array modelling, for example see [2], [3], [15]–[17]. Due to the principle of superposition, linear potential theory allows for the separation of the total wave field into the following components (Eq. (2)):

$$\varphi_t(x,y,z) = \varphi_i + \varphi_d + \sum_i^6 \varphi_r \tag{2}$$

where φ_t is the total velocity potential, φ_i is the incident wave potential, φ_d the diffracted wave potential and $\sum_i^6 \varphi_r$ is the sum of the radiated wave potentials for each degree of freedom of the device. In our investigation we also make use of the term perturbed wave to denote the wave resulting from sum of the diffracted and radiated potentials.

B. Boundary Element Method Solver

In our coupling approach the inter-array effects are resolved by simulating the WEC motions by the open-source potential flow Boundary Element Method (BEM) solver NEMOH. Given Eq. (1), NEMOH solves the Laplace equation Eq. (3) for the complex velocity potential φ:

$$\Delta\varphi = 0 \tag{3}$$

given a set of boundary conditions on the wetted body surface, the free surface, sea bottom and far field. The equations are solved by utilising the method of Green's functions, as reported in detain [11]. An important restriction imposed by the method is the assumption that the water depth h is constant throughout the inter-array domain. The free surface elevation η is calculated by taking the real part of the complex potential $\bar{\eta}$ that is in turn obtained in NEMOH from the free surface boundary condition Eq. (4). From the superposition principle, Eq. (2), free surface elevations η can be obtained separately for the WEC motions due to the diffracted and the radiated potentials.

$$\eta = -\frac{1}{g}\left(\frac{\partial\varphi}{\partial t}\right)_{z=0} \tag{4}$$

where g is the acceleration due to gravity and z is the vertical water velocity.

C. Mild-slope Wave Propagation Model

In simulating the far-field effects the wave propagation model MILDwave is employed [12], [13]. MILDwave, developed at the Coastal Engineering Research Group of Ghent University, Belgium, is a phase-resolving model based on the depth-integrated mild-slope equations (eqs. (5a) and (5b)) of Radder and Dingemans [18]. This particular model has been used in modelling WEC arrays in a number of recent publications [8], [9], [13], [19]. The mild-slope equations (eqs. (5a) and (5b)) are solved using a finite difference scheme that consists of a two-step space-centred, time-staggered computational grid, as detailed in [20].

$$\frac{\partial\eta}{\partial t} = \frac{\omega^2 - k^2 CC_g}{g}\varphi - \nabla\cdot\left(\frac{CC_g}{g}\nabla\varphi\right) \tag{5a}$$

$$\frac{\partial\varphi_t}{\partial t} = -g\eta \tag{5b}$$

Here η and φ are, respectively, the surface elevation and the total velocity potential at the free water surface, g is the gravitational acceleration, C is the phase velocity and C_g the group velocity for a wave with wave number k and angular frequency ω.

D. Coupling Methodology

In order to model the far-field effects in a timely manner with a reasonable accuracy, a one-way coupling methodology introduced in [9] is employed. In brief, the perturbed wave field is calculated in NEMOH and is propagated into MILDwave on a circle large enough to enclose the inter-array region that contains the WECs. In this analysis, the coupling radius r_c is equal to 100 m for both the flap and the buoy arrays. r_c is the circle on which the data from NEMOH is imported into MILDwave. The MILDwave gird resolution is set at Δx = Δy = 2 m. For further details on the coupling see [9].

E. Modelled WECs

1) Bottom-Fixed pitching flap: The first type of WEC investigated is a bottom-fixed flap driven by the surging motion of the waves. Currently such devices are only designed to be deployed in shallow waters at depths between 10 and 20 meters. Examples of this technology are the Oyster (Wave Energy Scotland), Wave Roller ™, and Resolute Marine Energy flap [21]. Our simulated device has the dimensions of 20 m width, 12 m height and 1 m thickness, with pitching

motion about the bottom end which is hinged to the seabed. The device is deployed at water depths of 10 m and thus its top side pierces the free surface. The Power Take-Off (PTO) of each WEC is modelled as a resistive damper in pitch with a coefficient value of $1.1 \times 10^8 kgs^{-2}$, which is representative of a resistive PTO tuned to maximise the energy absorption under a typical sea state of peak period equal to 8 seconds. For details on the equation of motion of the pitching flaps and the PTO coefficients applied see [22].

2) floating heaving buoy: The second type of WECs in this study is a flat circular cylinder with a diameter of 10 m and a draft of 2 m. The shape was selected based on its overall dimensions being similar to several promising WEC technologies, namely those of Seabased, Seatricity and Carnegie Wave [21]. All three devices are in the planning stages of a pre-commercial WEC array. The Power Take-Off (PTO) of each WEC is modelled as a resistive damper with a B_{PTO} value of $3.6 \times 10^5 kgs^{-2}$, which is representative for a resistive PTO of the WEC type we model [6]. Since a changing value of B_{PTO} depending on the wave frequency was not found to have a large impact on the device motion, for simplicity the PTO coefficient value is set constant for each of the WECs in an array. Further details can be found in [9].

F. WEC array layouts

The two WEC arrays are arranged in the same staggered configuration as shown in Fig. 1, which has the same crest-parallel width l_y of 120 m. The arrays are designed to have a comparable spatial extent of 30 m by 120 m, to allow a reference characteristic for comparison. The direction of the incoming waves, indicated by λ, is from the left. Here d_x and d_y are the x and y WEC centre-to-centre separation distances, respectively. This type of staggered configuration has been shown to maximize the absorbed wave power in numerical studies, for example in [1], and in experimental studies [23], [24] and is deemed a realistic representation of first-generation WEC arrays. This is also the type of array configuration that a number of studies [5], [25] have investigated for the effects of a wave array on the coastline. The arrays are first modelled over constant bathymetry, with the flap set at a depth of 10 m whilst the floating buoy in a depth of 20 m, with each device placed at a realistic deployment depth. Subsequently a variable bathymetry with a gentle slope of 2% is modelled as shown in Fig. 2, with the devices set at the locations of their respective deployment depths.

III. RESULTS

In this section we show the wave field around the two arrays that are displayed in Fig. 1 in Sec. II-F with the WEC types detailed in Sec. II-E. The results demonstrated herein are for a regular wave with wave height of 2 m and wave period equal to 6 s, 8 s, and 10 s. The basin is square with the length and width equal to 2000 m. In all subsequent contour plots and profiles we present the absolute value of the wave elevation $|\eta|$ that shows the modification of the wave field due to the presence of the array.

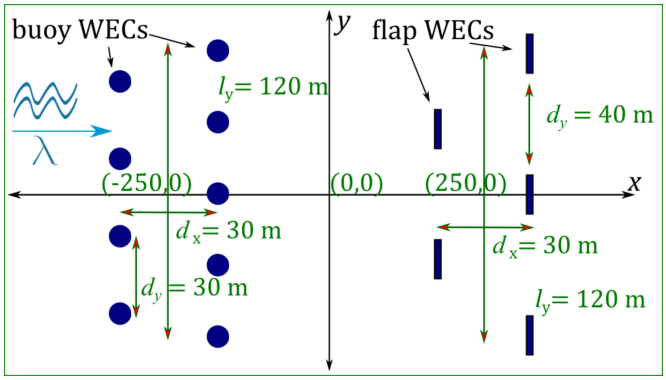

Fig. 1: x-y PLANE (TOP) VIEW OF THE ARRAY LAYOUT FOR 9 HEAVING BUOYS AND 5 PITCHING FLAPS. λ IS THE INCOMING WAVE.'

A. Far-field effects for a fixed water depth

We begin our overview of the results by focusing on the difference in the *far-field* effects of the two types of WEC arrays. To achieve this we place each array on a flat sea bottom, with the buoys located at a constant water depth of 20 m and the flaps at a constant depth of 10 m. The results in the form of contour plots of $|\eta|$ for the array of buoys are shown in Fig. 3 while those for the flaps are displayed in Fig. 4 for H = 2 m and T = 6, 8, and 10 seconds, from left to right. Note that the location of the buoy and flap arrays, in indicated by the red boxes on the images, is different for the two array types as explained in Sec. II-F. We note a significant difference of the *far-field* effects between the heaving buoy and the pitching flap arrays. For the buoys there is a significant decrease in the magnitude of the *far-field* effects between T = 6 s and T = 8 and 10 seconds with the magnitude of the latter being less than the 5% significance threshold everywhere outside of the inner domain, that is the zone immediately outside the coupling radius r_c. This is in large part due to the decreasing motion of the WECs as the wave period moves away from the resonance period of $T_r = 4.6$ s. By way of contrast, the modification of the wave field around the flaps is significant for all three wave periods studied. The maximum increases in $|\eta|$ range from 20 % for T = 8 to almost 30 % for T = 10 s and T = 6 s. The lowest minimum in the wake zone is found at T = 6 s in the region immediately outside of r_c where the wave amplitude decrease by almost 35 %. We can define the wake zone as the region of reduced $|\eta|$ in lee of the array. As we can inspect in Fig. 4 this wave zone extends out as far as 800 m in lee of the array for T = 6 s. It is interesting to note that the wave augmentation and reduction does not follow the same trend with increasing wave period. As we increase the wave period, the wake effect, that is the region with an appreciable decrease in $|\eta|$ in lee of the array gets smaller. In opposition, the mean wave height in front of the array actually increases with an increment in wave period.

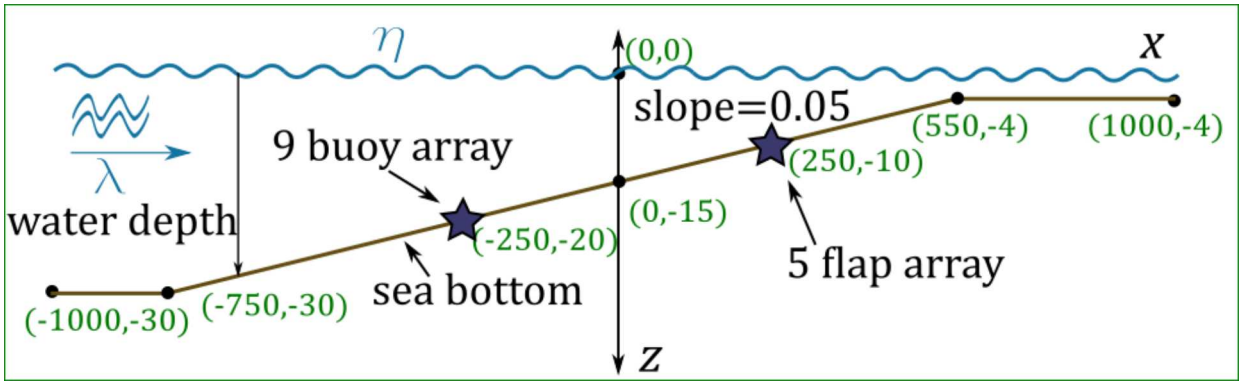

Fig. 2: DEPTH PROFILE SHOWING THE LOCATION OF THE TWO MODELLED ARRAYS. x-z PLANE (SIDE) VIEW. THE COASTLINE IS LOCATED AT THE RIGHT SIDE OF HE FIGURE.

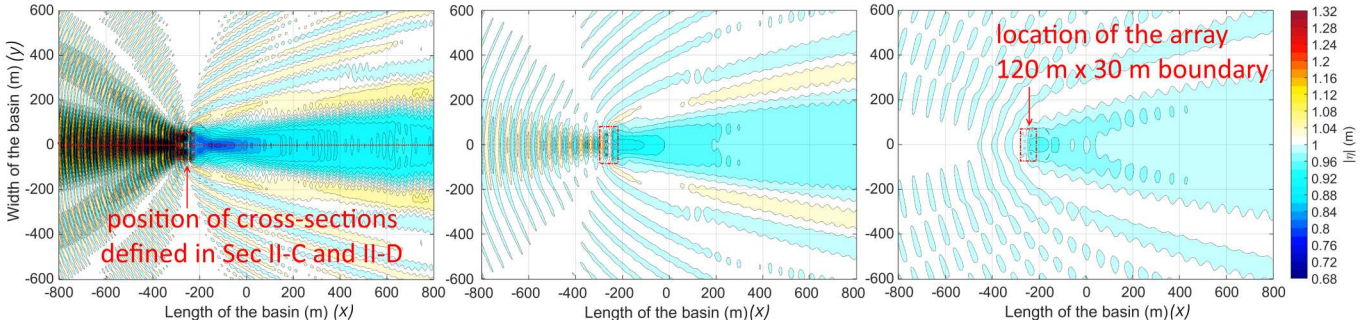

Fig. 3: COUPLED $|\eta|$ VALUES FOR AN ARRAY OF 9 STAGGERED HEAVING BUOYS FOR T = 6 s (LEFT), T = 8 s (CENTRE) AND T = 10 s (RIGHT).THE WATER DEPTH IS 20 m. WAVES ARE PROPAGATING FROM LEFT TO RIGHT.

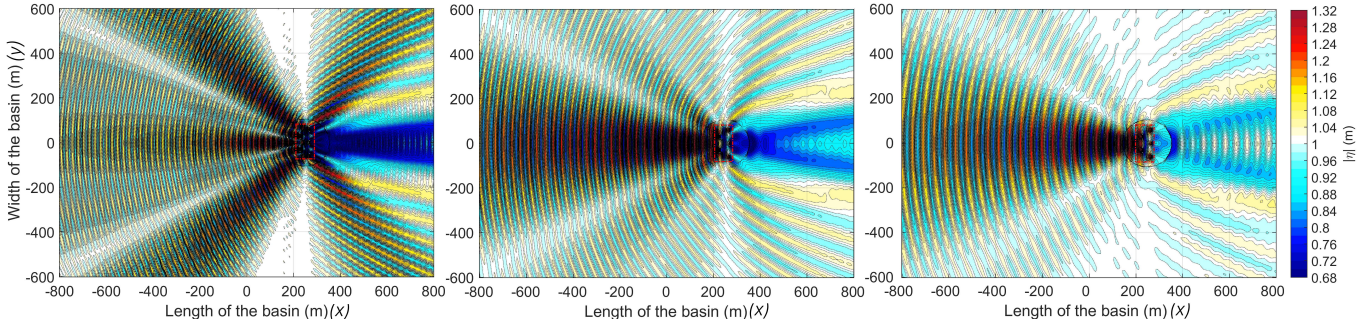

Fig. 4: COUPLED $|\eta|$ VALUES FOR AN ARRAY OF 5 STAGGERED PITCHING FLAPS FOR T = 6 s (LEFT), T = 8 s (CENTRE) AND T = 10 s (RIGHT).THE WATER DEPTH IS 10 m. WAVES ARE PROPAGATING FROM LEFT TO RIGHT.

B. Far-field effects on a sloping sea bottom

Next, we turn our attention to modelling the two WEC arrays for a variable sea bottom, where we compare the magnitude of the *far-field* effects to the influence of shoaling effects on the wave field. The modelled sea bottom is sketched out in Fig. 2. Note that the 9-buoy array is placed at 20 m while the 5-flap array is located at a 10 m water depth. Therefore the location of the former is 250 m offshore while the later is located 750 m offshore with regard to the coastline (see Fig. 2). This represents a realistic deployment location for both types of devices, as both the flap and the heaving buoy have practical deployment depth ranges. In Fig. 5 we observe the wave field for a 9 WEC array of bottom fixed flaps for T = 6 s, T = 8 s, and T = 10 s, fixed at a 10 m depth. We note that as for the fixed sea bottom case in Sec. III-A, the *far-field* effects dramatically decrease from a wave of T = 6 s to the other two wave periods modelled. Concurrently, as expected, the shoaling due to the decreased depth becomes significant for a longer wave length. Only at T = 6 s does the array wave field modification outweigh the shoaling effects at the right side of

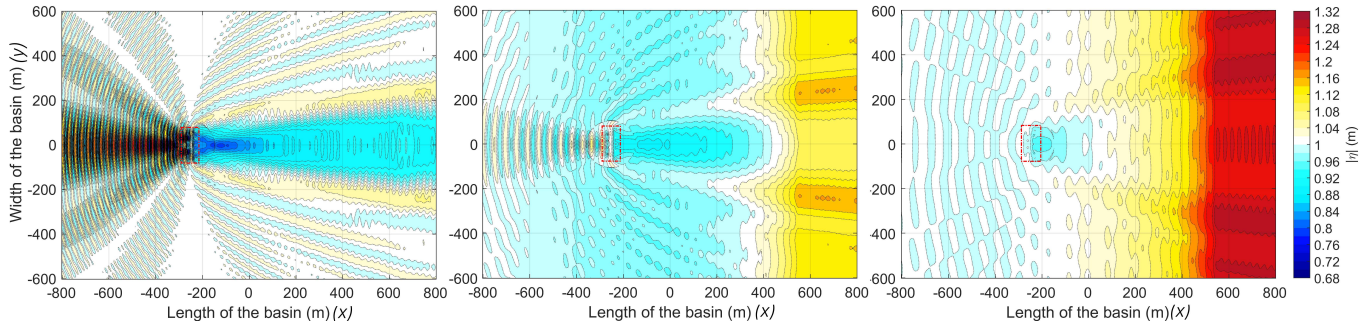

Fig. 5: COUPLED $|\eta|$ FOR AN ARRAY OF 9 STAGGERED HEAVING BUOYS FOR T = 6 s (LEFT), T = 8 s (CENTRE) AND T = 10 s (RIGHT) ON A SLOPING BATHYMETRY. WAVES ARE PROPAGATING FROM LEFT TO RIGHT.

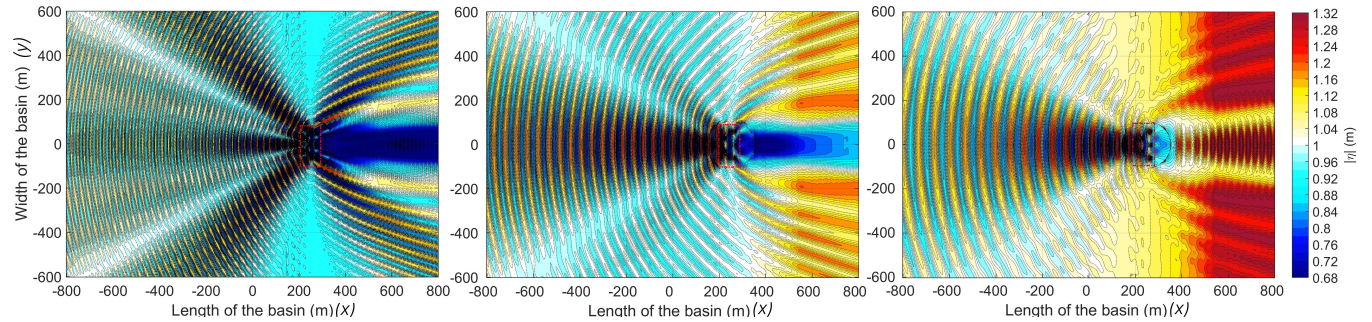

Fig. 6: COUPLED $|\eta|$ FOR AN ARRAY OF 5 STAGGERED PITCHING FLAPS FOR T = 6 s (LEFT), T = 8 s (CENTRE) AND T = 10 s (RIGHT) ON A SLOPING BATHYMETRY WAVES ARE PROPAGATING FROM LEFT TO RIGHT.

the domain. In this case, the wave modification is significant both upwave and downwave of the buoy array. For the wave of T = 8 and T = 10 seconds, in contrast, the influence of the array on the near-shore region down-wave of the array is practically nil, while the shoaling effect is significant. For the case of variable bathymetry, the difference between the 9-buoy and the 5-flap array is even more pronounced. In Fig. 6, we note a significant interaction between the *far-field* effects of the array and the shallow water transformation of waves of 8 and 10 seconds. Unlike the case of the buoys, the flaps exact a considerable influence on the near-shore zone, with a reduction in the amplitude of the incident wave directly in lee of the array. Also of note is the augmentation of the reflection immediately upwave of the array and a reduction in the reflection farther away upwave, compared with the flat bottom scenario modelled in Fig. 4. At the same time, because of wave dispersion, the comparative magnitude at the sides of the flap array decreases in relation to the flat bottom case. Regardless, it is apparent that for the case of the 5-flap array the *far-field* effects are significant for the entire spectrum of waves modelled.

C. Assessing the influence of a sloping sea bottom

It is instructive to look at the $|\eta|$ values along a cross section at $y = 0$ or across the symmetric axis of the array parallel to the incoming wave ($x - axis$), and to compare the effects of a sloping bathymetry on the $|\eta|$ upwave and downwave of the WEC array. In figs. 7 to 9 we show these cross sections for an array of 9 buoys for and T = 6 s, 8 s, and 10 s, respectively. The same cross sections for the array of 5 pitching flaps are displayed in figs. 10 to 12 for wave periods of 6 s 8 s, and 10 s. The position of the cross-section is indicated using a red dashed line in Fig. 3, and is the same for all the various cases displayed in this subsection. Note the location of the buoy array marked by the green boxes with Ⓑ and the flap array marked with Ⓕ . The incident wave height is 2 m. In these cross-sections we can clearly observe the trends noted in Sec. III-B in relation to the difference in the magnitude of change in $|\eta|$ and in the trends of the *far-field* effects of the arrays. We can also better discern the difference in the effect of the sloping bathymetry for a given device type and wave period. For example, in Fig. 8 and Fig. 9, we note how the effect of the bathymetry easily outweighs the wake effects in lee of the buoy array for T = 6 s and T = 8 s. At the same time for both T = 6 s (Fig. 7) and T = 8 s (Fig. 8) the effects of the buoy array upwave are significant compared to the effects of the sloping sea floor with the only influence of the latter being a shift in phase.

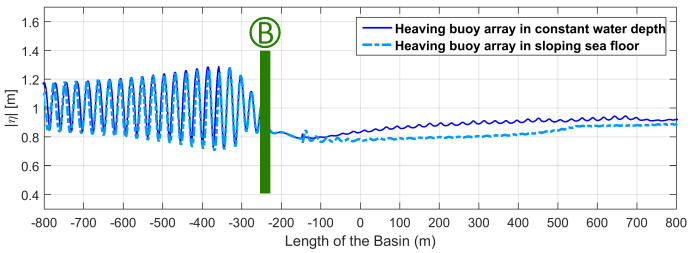

Fig. 7: CROSS-SECTION OF $|\eta|$ ACROSS $y = 0$ FOR AN ARRAY OF 9 STAGGERED HEAVING BUOYS FOR H = 2 m T = 6 s.

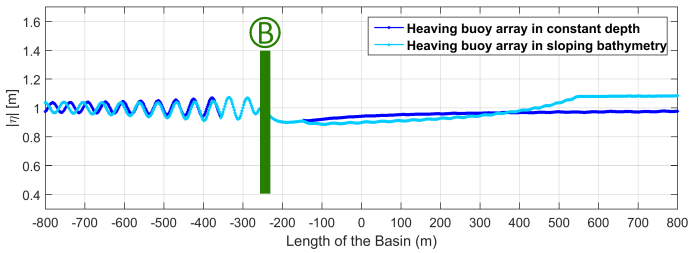

Fig. 8: CROSS-SECTION OF $|\eta|$ ACROSS $y = 0$ FOR AN ARRAY OF 9 STAGGERED HEAVING BUOYS FOR H = 2 m T = 8 s.

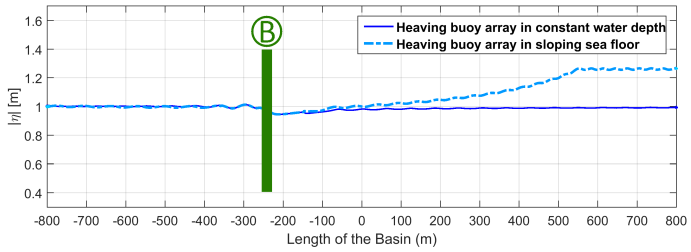

Fig. 9: CROSS-SECTION OF $|\eta|$ ACROSS $y = 0$ FOR AN ARRAY OF 9 STAGGERED HEAVING BUOYS FOR H = 2 m T = 10 s.

For the flaps, the situation is quite distinct, in that the flap array effects upwave and downwave are both significantly modified by the sloping bathymetry, especially for T = 8 s (Fig. 11) and T = 10 s (Fig. 12). In the latter, we see a significant increase in the overall wave elevation as we move closer to shore. An increment is also observed in the wave elevation in the wake zone behind the array on a sloping bathymetry compared to its counterpart at a constant water depth, counter to what occurs for T = 6 s and T = 8 s. Also note the magnification of the amplitude of the wake effects, both in front and in lee of the flap array in this particular case. We note that in our simulated basin as shown in Fig. 2 the smallest depth is 4 m. This is deeper than the wave breaking limit for the H = 2 m, T = 6 s, T = 8, and T = 10 s waves modelled. Therefore, the wave breaking mode in MILDwave, as detailed in [10], is not implemented.

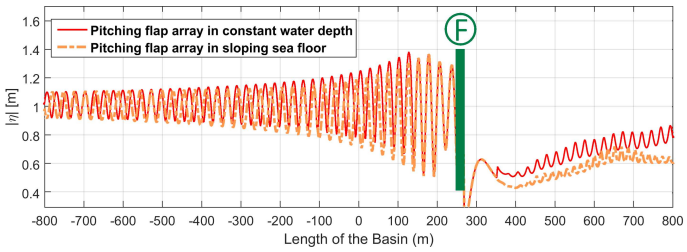

Fig. 10: CROSS-SECTION OF $|\eta|$ ACROSS $y = 0$ FOR AN ARRAY OF 5 STAGGERED PITCHING FLAPS FOR H = 2 m T = 6 s.

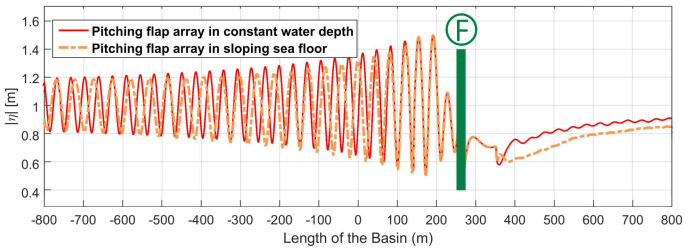

Fig. 11: CROSS-SECTION OF $|\eta|$ ACROSS $y = 0$ FOR AN ARRAY OF 5 STAGGERED PITCHING FLAPS FOR H = 2 m T = 8 s.

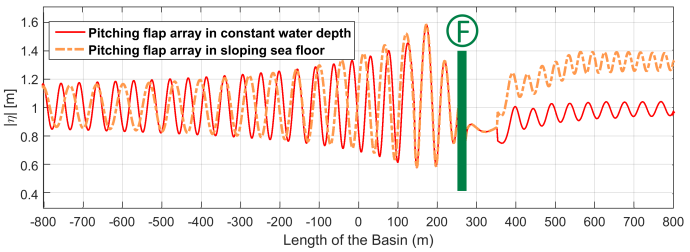

Fig. 12: CROSS-SECTION OF $|\eta|$ ACROSS $y = 0$ FOR AN ARRAY OF 5 STAGGERED PITCHING FLAPS FOR H = 2 m T = 10 s.

D. Comparing the magnitude of the array effects for a constant depth to those for sloping sea bottom

In addition to interpreting the influence of the sloping bathymetry on the *far-field* effects, by plotting the magnitude of $|\eta|$ for both the heaving buoy array and the pitching flap array for the case of sloping bathymetry, we can quantify the difference in the magnitude of the array effects. These differences have practical implications as we will examine in Sec. IV. In figs. 13 to 15 we plot $|\eta|$ at $y = 0$ on sloping bathymetry for the two types of WECs. Again, the large contrast in the magnitude and extend of the flaps' modifications of the wave field are apparent in figs. 13 to 15. The only case where the interactions of the two WEC types are comparable is for the case of T = 6 s, and only in front of the array where we observe that the buoy and the flap modify the wave field by 20 %. Still, downwave of the 5-flap array, the

impact is significantly greater, with up to a 60 % reduction in $|\eta|$ behind the array. For the buoy array the decrease is only 20 % although for this modelled wave period the extent of this decrease is quite large, up to 600 m in lee of the bouy array. For T = 8 s in Fig. 14, the difference is pronounced. The presence of the buoy array reduces the wave height downwave by no more than 10 % for about 500 m, after which the increase in the wave height due to the shoaling negates this effect. In contrast, $|\eta|$ behind the flap array is reduced by 40 % and the reduction is marked, notwithstanding the shoaling effect all the way to the end of the numerical wave basin. A part of this effect is a consequence of the B_{PTO} value which is optimised for T = 8, enhancing the device motion, as explained in Sec. II-E1. For T = 10 s shown in Fig. 15, we note that in lee of the arrays the effect of depth reduction outweighs the effect of the array wave energy absorption for both cases. The effect of the buoy array in modifying $|\eta|$ can be seen as negligible. On the contrary, for the flap array we note significant modifications of $|\eta|$ both upwave and downwave of the array. At this wave period the strong interactions are not unexpected, since the resonance period of the flap is close to 10 seconds. Upwave, we observe a significant modulation in the wave field due to reflection, with an up to 80 % variation between the peak and trough amplitude. This is significant as the wave field in front of the flap array is quite disturbed with ramifications for any other WECs placed in that area or indeed for shipping activities. Downwave we note a slight reduction in the amplitude before it is overtaken by the augmentation of the wave due to shoaling.

IV. DISCUSSION

A. *Quantifying the difference in the far-field effects of the two WEC types*

Based on the evidence presented in Sec. III we can see that the *far-field* effects of the array of 5 flaps are much greater than those of the heaving buoys, for all wave periods considered for both the flat and sloping bathymetry. This was expected, given the fact that the flaps are modelled as bodies which take up the entire water column. Therefore, we would expect a significant effect, especially as the waves transform in the transition from deep water to shallow water and their surge energy flux component becomes more significant. Moreover, unlike the heaving buoys, the flaps are not designed to be working in resonance, consequently, their wider energy-capturing bandwidth encompasses the entire range of periods studied. This is consistent with a previous investigation by Borgarino et al. [26] which compared the *far-field* effects of an array of heaving buoys to that of barges. While the floating barge and the pitching flap differ in principle of operation, their modelled counterparts as presented in this work and in [26] are quite similar under the assumptions of linearity. As a consequence in our work we observe a similar magnitude and extent of difference between the modifying effect of the two different arrays. Note that unlike in this investigation the aforementioned study utilized a BEM code for the entire modelling domain and did not include the modifying effects of bathymetry.

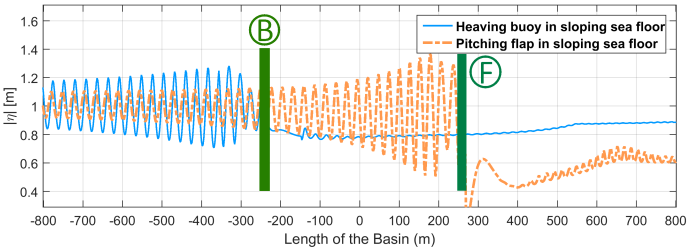

Fig. 13: CROSS-SECTION OF $|\eta|$ ACROSS $y = 0$ FOR AN ARRAY OF 9 STAGGERED HEAVING BUOYS (B) AND AN ARRAY OF 5 STAGGERED PITCHING FLAPS (F) FOR H = 2 m T = 6 s.

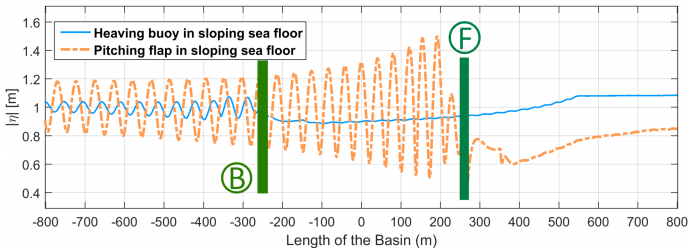

Fig. 14: CROSS-SECTION OF $|\eta|$ ACROSS $y = 0$ FOR AN ARRAY OF 9 STAGGERED HEAVING BUOYS (B) AND AN ARRAY OF 5 STAGGERED PITCHING FLAPS (F) FOR H = 2 m T = 8 s.

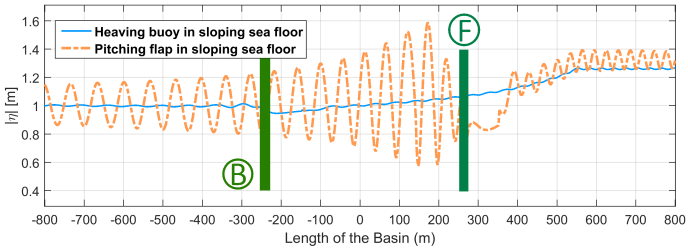

Fig. 15: CROSS-SECTION OF $|\eta|$ ACROSS $y = 0$ FOR AN ARRAY OF 9 STAGGERED HEAVING BUOYS (B) AND AN ARRAY OF 5 STAGGERED PITCHING FLAPS (F) FOR H = 2 m T = 10 s.

A study similar in scope and methodology to ours was performed by Charrayre *et al.* [6] where a staggered array of 11 devices was modelled over a gently sloping bathymetry using a coupling between a BEM code and a wave propagation model. This particular study simulated heaving buoys of equal radius and draft of 10 m in T = 8 s regular waves and concluded that for the scenario modelled the effect of the WEC array in the near-shore region 2000 m away from the location of the array was negligible. As in our investigation,

they have found the sloping bathymetry to slightly decrease the amplitude of the perturbed wave field up-wave or in front of the array and increase it down-wave or in lee of the WECs. This amounts to an overall lessening of the impact This observed change is quite small however, and for the period studied, the authors consider it negligible, corroborating with our observations of similar data in the second panel in Fig. 3. Note however, that for the pitching flaps, the effect is much stronger and certainly cannot be neglected.

B. Implications for modelling the impact of an array of WECs on a coastal region

Since wave energy projects are almost assuredly going to be located close to the coastline for logistical and economic reasons, the chief aim of studies investigating the *far-field* effects of an array or a farm of WECs is to deduce the impacts of a wave energy project on the surrounding coast. Several studies have been performed to this end, including [5], [25], [27]–[29]. These studies have looked at a regional scale impact of wave farms on a coastline. Because of the large domain, these investigations have modelled WEC arrays using phase-averaged spectral models.

Most of the studies investigating WEC arrays using phase-averaging models define the WEC as an obstacle with a fixed transmission coefficient [27] which is determined via numerical models or tank testing. However this transmission coefficient is not frequency dependent and does not correctly represent the absorption of a real WEC. We can observe this clearly in the magnitude of the difference in the *far-field* effects between the three periods in Figs. 5 and 6, or in the cross-sections in figs. 7 to 9 and figs. 10 to 12 for the buoys and the flaps, respectively. Because our coupling methodology allows us to correctly model the frequency dependence of the diffraction and absorption of the wave by the WEC array, it avoids this limitation of phase-resolving spectral models. Moreover, because the spectral models are depth averaged at the source, differences such as those we observe between the flat buoys, which have a small refraction effects, versus the flaps, for which the effect is much greater, are able to be differentiated. At the same time, the wave propagation model to which we couple the depth-dependent near field result allows us to propagate these frequency and depth dependent effects over large enough areas to be able to gauge the impact on the coastline at scales similar to that investigated in [27], [29] or [5], [25]. It also allows us to model wave transformation processes in very shallow areas. As mentioned in Sec. III-C, MILDwave allows for the possibility of including effects of wave breaking in the simulations. Whilst wave energy devices are not likely to be placed in the wave breaking zone, their wake effects can certainly impact the wave breaking process, especially when the effect is significant as in the case of flap arrays.

V. CONCLUSIONS AND FUTURE WORK

In this paper we have seen how the coupled methodology between a BEM model and a wave propagation model allows us to ascertain the essential differences in the *far-field* effects between an array of heaving buoys and pitching flaps. We have observed that the effect of the heaving buoy array is much more limited in frequency and spatial extent. We have also seen a much greater effect of the heaving flaps on a shallow coastal zone, in a basin with a sloped bathymetry. We should note here that in order to present a realistic scenario, the buoy and flap arrays are not co-located, as is noted in Fig. 2. Therefore, we would expect the *wake effect* of the pitching flaps to be greater regardless of the modelling scenario because they are closer to the modelled 'coast'. In our view, however, this is a fair comparison as we have to remember that given their respective deployment depth restriction, the pitching flaps will always be placed closer to the coast, thereby magnifying their effect. We have observed in the flat bathymetry case, the effects of the flap array are compounded by the wide absorption bandwidth and large cross-wave area of each flap. Therefore, we can conclude that an array of pitching flaps will need to be carefully evaluated for the potential effect on the coastline. Conversely, an array of heaving buoys controlled by passive restive PTO will have a negligible effect on the surrounding areas. Again, this is not surprising as the primary means by which these device modify the surrounding field is radiation which falls off as $1/r$, where r is the radial distance away from the buoy centre. Similar conclusion have been made in studies such as [30] and [6]. It is not difficult to extend this conclusion to observe that the phase-averaging models discussed in Sec. IV are more appropriate for modelling an array of pitching flaps than heaving buoys. Still, the frequency distribution of wave array effects is important, especially as littoral processes such as sediment transport and wave-current interactions are strongly frequency-dependent. As such, the new coupling methodology utilised in this investigation is an important addition to the numerical toolbox of wave energy developers and coastal scientists. In this investigation we have focused on a narrow subset of modelling scenarios that give us good insight into the difference in the *far-field* effects between a flap and a buoy array. However, we have only simulated a small subset of possibilities. Therefore, the next steps in our modelling work is to extend the methodology to irregular waves, whereby we can model a realistic wave climate, similar to what has been performed with spectral models in [4], [5], [28]. For our linear coupling strategy, this is a matter of summing up the effects at each frequency given a particular input wave spectrum. Furthermore, we will consider different array configurations and even more importantly, different ways of modelling the PTO that would more accurately represent the absorption by the current crop of heaving devices. Finally, as we have pointed out in Sec. IV, our eventual aim is place the WEC arrays in a basin in MILDwave that mimics a real coastline. Since MILDwave is fully capable of modelling coastal transformation processes, we will be able to deduce the impact of a wave farm on any particular area given a device type and the devices' location relative to the coast.

ACKNOWLEDGEMENT

This research is being supported by the Research Foundation Flanders (FWO), Belgium - FWO.OPR.2.0 - FWO research project No. 3G029114.

REFERENCES

[1] B. Child and V. Venugopal, "Optimal configurations of wave energy devices," *Ocean Engineering*, vol. 37, pp. 1402–1417, 2010.

[2] P. B. Garcia Rosa, G. Bacelli, and J. Ringwood, "Control-informed optimal layout for wave farms," *IEEE Transactions on Sustainable Energy*, vol. 6, pp. 575–582, 2015.

[3] C. Sharp and B. L. DuPont, "Wave energy converter array optimization: A review of current work and preliminary results of a genetic algorithm approach introducing cost factors," in *41st Design Automation Conf., ASME Int'l Design Engineering Technical Conf. Boston, MA, USA. August 2-5.*, 2015.

[4] H. Smith, C. Pearce, and D. Millar, "Further analysis of change in nearshore wave climate due to an offshore wave farm: An enhanced case study for the wave hub site," *Renewable Energy*, vol. 40, no. 1, pp. 51–64, 2012.

[5] G. Iglesias and R. Carballo, "Wave farm impact: The role of farm-to-coast distance," *Renewable Energy*, vol. 69, pp. 375 – 385, 2014. [Online]. Available: http://www.sciencedirect.com/science/article/pii/S0960148114002341

[6] F. Charrayre, C. Peyrard, M. Benoit, and A. Babarit, "A coupled methodology for wave-body interactions at the scale of a farm of wave energy converters including irregular bathymetry," in *Proc. of the ASME 2014 33rd Int'l Conference on Ocean, Offshore and Arctic Engineering June 8-13, 2014, San Francisco, CA, USA*, 2014.

[7] N. Tomey-Bozo, J. Murphy, T. Lewis, P. Troch, and G. Thomas, "Flap type wave energy converter modelling into a time-dependent mild-slope equation model," in *Proc. of the 2nd Int'l Conference on Offshore Renewable Energies*, 2016, pp. 277–284.

[8] T. Verbrugghe, P. Troch, A. Kortenhaus, V. Stratigaki, and A. Engsig-Karup, "Development of a numerical modelling tool for combined near and far field wave transformations using a coupling of potential flow solvers," in *Proc. of the 2nd Int'l Conference on Renewable Energies Offshore 24 - 26 October 2016, Lisbon, Portugal*, 2016.

[9] P. Balitsky, G. Verao Fernandez, V. Stratigaki, and P. Troch, "Coupling methodology for modelling the near-field and far-field effects of a wave energy converter," in *Proceedings of the ASME 36th International Conference on Ocean, Offshore and Arctic Engineering (OMAE2017)*, 2017.

[10] V. Stratigaki, "Experimental study and numerical modelling of intra-array interactions and extra-array effects of wave energy converter arrays," 2014.

[11] A. Babarit and G. Delhommeau, "Theoretical and numerical aspects of the open source bem solver NEMOH," in *Proc. of the 11th European Wave and Tidal Energy Conference 6-11th Sept 2015, Nantes, France*, 2015.

[12] P. Troch, "MILDwave - a numerical model for propagation and transformation of linear water waves." Department of Civil Engineering, Ghent University, Ghent. Internal Report., Tech. Rep., 1998.

[13] P. Troch and V. Stratigaki, "Phase-resolving wave propagation array models," in *Numerical Modelling of Wave Energy Converters*, M. Folley, Ed. Elsevier, 2016, ch. 10, pp. 191–216.

[14] M. Alves, "Wave energy converter modelling techniques based on linear hydrodynamic theory," in *Numerical Modelling of Wave Energy Converters*, M. Folley, Ed. Elsevier, 2016, ch. 1, pp. 11–65.

[15] A. Babarit, "On the park effect in arrays of oscillating wave energy converters," *Renewable Energy*, vol. 58, pp. 68–78, 2013.

[16] H. Wolgamot, P. Taylor, and R. Eatock Taylor, "The interaction factor and directionality in wave energy arrays," *Ocean Engineering*, vol. 47, pp. 65–73, 2012.

[17] C. McNatt, V. Venugopal, and D. Forehand, "The cylindrical wave field of wave energy converters," *Int'l Journal of Marine Energy*, vol. 3, pp. 26–39, 2013.

[18] A. Radder and M. Dingemans, "Canonical equations for almost periodic, weakly nonlinear gravity waves," *Wave Motion*, vol. 7, no. 7, pp. 473–485, 1985.

[19] C. Beels, P. Troch, G. D. Backer, M. Vantorre, and J. D. Rouck, "Numerical implementation and sensitivity analysis of a wave energy converter in a time-dependent mild-slope equation model," *Coastal Engineering*, vol. 57, no. 5, pp. 471 – 492, 2010. [Online]. Available: http://www.sciencedirect.com/science/article/pii/S0378383909001823

[20] M. Brorsen and J. Helm-Petersen, "On the reflection of short-crested waves in numerical models," in *Proc. of the 26th Int'l Conference on Coastal Engineering, Copenhagen*, 1998, pp. 394–407.

[21] National Renewable Energy Laboratory. (2017) Marine and hydrokinetic technology database. [Online]. Available: http://en.openei.org/wiki/Marine_and_Hydrokinetic_Technology_Database

[22] N. Tomey-Bozo, J. M. A. Babarit, P. Troch, T. Lewis, and G. Thomas, "Wake effect assesment of a flap-type wave energy converter farm using a coupling methodology," in *Proceedings of the ASME 36th International Conference on Ocean, Offshore and Arctic Engineering (OMAE2017*, 2017.

[23] V. Stratigaki, P. Troch, T. Stallard, J. Forehand, D.and Kofoed, M. a. Folley, M. Benoit, A. Babarit, and J. Kirkegaard, "Wave basin experiments with large wave energy converter arrays to study interactions between the converters and effects on other users," *Energies*, vol. 7, pp. 701–734, 2014.

[24] V. Stratigaki, P. Troch, T. Stallard, D. Forehand, M. Folley, J. Kofoed, M. Benoit, A. Babarit, M. Vantorre, and J. Kirkegaard, "Sea-state modification and heaving float interaction factors from physical modelling of arrays of wave energy converters," *Journal of Renewable and Sustainable Energy*, vol. 7, no. 7, 2015. [Online]. Available: http://dx.doi.org/10.1063/1.4938030

[25] J. Abanades, D. Greaves, and G. Iglesias, "Wave farm impact on the beach profile: A case study," *Coastal Engineering*, vol. 86, pp. 36 – 44, 2014. [Online]. Available: http://www.sciencedirect.com/science/article/pii/S0378383914000179

[26] B. Borgarino, A. Babarit, and P. Ferrant, "Impact of the separating distance between interacting wave energy converters on the overall energy extraction of an array," in *Proceedings of the 9th European Wave 1 Tidal Energy Conference, Southampton, UK*, 2011.

[27] D. Millar, H. Smith, and D. Reeve, "Modelling analysis of the sensitivity of shoreline change to a wave farm," *Ocean Engineering*, vol. 34, no. 56, pp. 884 – 901, 2007. [Online]. Available: http://www.sciencedirect.com/science/article/pii/S0029801806001272

[28] V. Venugopal and G. Smith, "Wave climate investigation for an array of wave power devices," in *7th European Wave and Tidal Energy Conference*, Porto, Portugal, 01/07 2007, p. 10.

[29] H. Smith, M. DL, and R. DE., "Generalisation of wave farm impact assessment on inshore wave climate, 7th european wave and tidal energy conference, porto, 11th - 14th sep 2007." in *Proc. of 7th European Wave and Tidal Energy Conference, Porto, 11th - 14th Sep 2007.*, 2007.

[30] B. Borgarino, A. Babarit, and P. Ferrant, "Impact of wave interaction effects on energy absorbtion in large arrays of wave energy converters," *Ocean Engineering*, vol. 41, p. 7988, 2012.